ACS NANO

www.acsnano.org

ARTICLE

Self-Destructive Structural Color Liquids for Time–Temperature Indicating

Chao Huang, Yuanyuan Shang, Jiachuan Hua, Yadong Yin,* and Xuemin Du*

Cite This: *ACS Nano* 2023, 17, 10269–10279

Read Online

ACCESS | Metrics & More | Article Recommendations | Supporting Information

ABSTRACT: **Vaccines are undoubtedly a powerful weapon in our fight against global pandemics, as demonstrated in the recent COVID-19 case, yet they often face significant challenges in reliable cold chain transport. Despite extensive efforts to monitor their time–temperature history, current time–temperature indicators (TTIs) suffer from limited reliability and stability, such as difficulty in avoiding human intervention, inapplicable to subzero temperatures, narrow tracking temperature ranges, or susceptibility to photobleaching. Herein, we develop a class of structural color materials that harnesses dual merits of fluidic nature and structural color, enabling thermal-triggered visible color destruction based on triggering agent-diffusion-induced irreversible disassembly of liquid colloidal photonic crystals for indicating the time–temperature history of the cold chain transport. These self-destructive structural color liquids (SCLs) exhibit inherent irreversibility, superior sensitivity, tunable self-destructive time (minutes to days), and a wide tracking temperature range (−70 to +37 °C). Such self-destructive SCLs can be conveniently packaged into flexible TTIs for monitoring the storage and exposure status of diverse vaccines *via* naked-eye inspection or mobile phone scanning. By overcoming the shortcomings inherent in conventional TTIs and responsive photonic crystals, these self-destructive SCLs can increase their compatibility with cold chain transport and hold promise for the development and application of the next-generation intelligent TTIs and photonic crystals.**

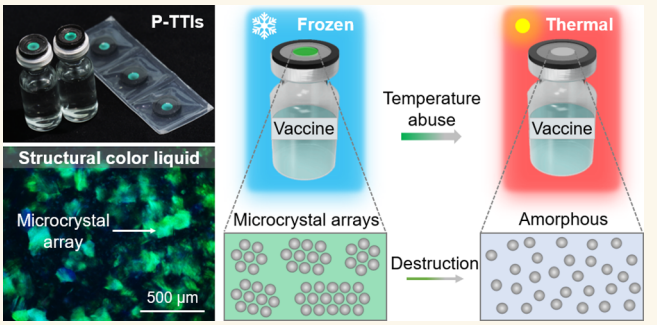

KEYWORDS: *photonic crystal, structural color, self-destruction, thermal responsive, time–temperature indicator*

INTRODUCTION

According to the World Health Organization (WHO), the coronavirus pandemic (COVID-19) has infected approximately 621 million people around the world, with more than 6.5 million deaths reported on October 16, 2022, ruining not only lives but also the economies.[1] Fortunately, the emerging COVID-19 vaccines have come to light as a powerful weapon in fighting the global pandemic. According to the United Nations' global vaccine strategy, at least 11 billion vaccine doses are required to end the pandemic ravages. To ensure that fully potent vaccines can reach target populations in good conditions, they must be transported through a cold chain that meets stringent requirements.[2,3] Conventional vaccines need to be stored at 2–8 °C, while the messenger ribonucleic acid (mRNA) vaccines must be frozen at subzero temperatures to avoid degradation.[4] In particular, the Moderna and Pfizer-BioNTech vaccines must be kept at −20 and −70 °C, respectively, throughout transportation, distribution, and storage. However, vaccines may be exposed to abnormal temperatures unwittingly due to operational errors or accidents. Once the exposure temperature and time deviate from the current regulatory standards, they may rapidly deteriorate, leading to reduced protection against diseases and even serious side effects.[4−6] Thus, time–temperature monitoring plays a vital role in decreasing the risk of subpotent vaccines and ensuring a reliable vaccine supply chain.

Time–temperature indicators (TTIs) based on electronics and various materials have been developed to indicate the accumulated influence of time–temperature history on the quality of products.[7−9] Although electronic TTIs can monitor the time–temperature information *via* wireless antenna sensors, they suffer from inevitable human intervention and generate a noticeable amount of electronic waste.[10] As a new paradigm, material-based TTIs provide convenient visual information on the time–temperature history *via* chemical reactions or dye diffusion of active additives (chemical reactants, microorganisms, enzymes, or dyes), raising consum-

Received: January 16, 2023
Accepted: May 9, 2023
Published: May 31, 2023

https://doi.org/10.1021/acsnano.3c00467
ACS Nano 2023, 17, 10269–10279

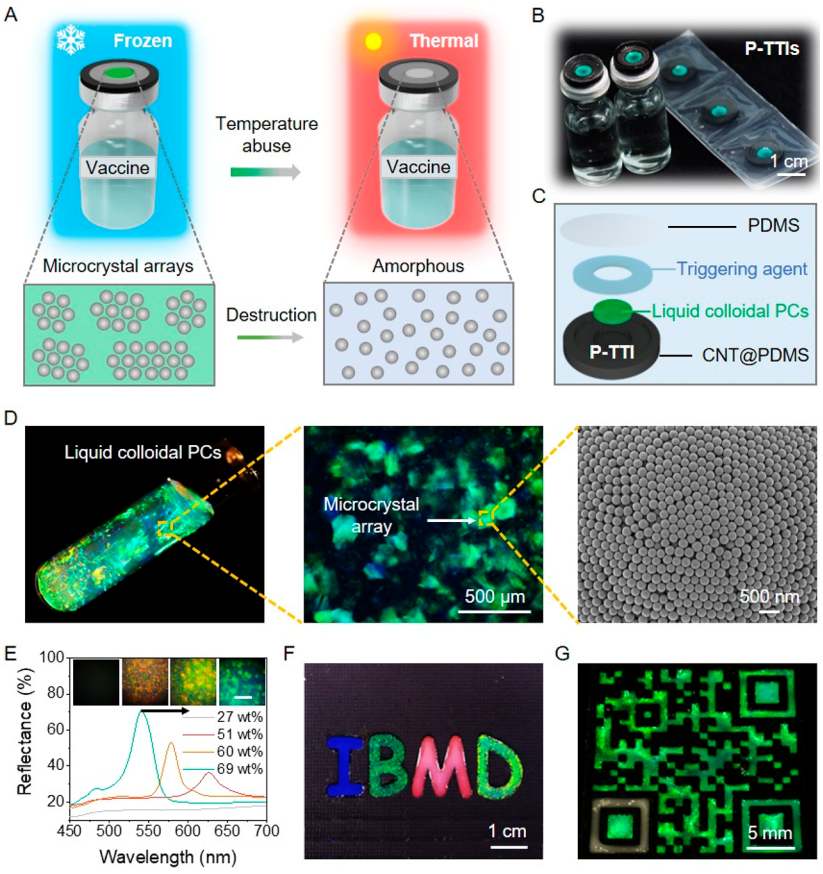

Figure 1. Fabrication of self-destructive structural color liquids. (A) Schematic illustration of thermal-triggered structural color destruction based on triggering agent-diffusion-induced irreversible disassembly of liquid colloidal PCs for indicating the time−temperature history of the vaccine. (B) Photography of packaged P-TTIs and P-TTIs adhered onto the caps of vaccine vials. (C) Schematic illustration of the structure of a P-TTI (carbon nanotubes, CNT; polydimethylsiloxane, PDMS). (D) Photograph, optical microscopic, and SEM images of the liquid colloidal PCs, the microcrystal arrays, and the enlarged surface morphology of the nonclose-packed colloidal crystal array. The liquid colloidal PCs have been stably stored at room temperature for 180 days. (E) Reflectance spectra and the corresponding optical microscopic images of the liquid colloidal PCs with different particle concentrations. By decreasing the particle concentration from 69 to 51 to 27 wt %, the structural color of liquid colloidal PCs shifts from green to red to colorless as evidenced by the corresponding Bragg reflection. Scale bar: 500 μm. (F) "IBMD" letters patterned with liquid colloidal PCs of various particle sizes (173, 190, 235, and 202 nm). (G) QR code patterned with green liquid colloidal PCs and a white triggering agent.

ers' awareness and avoiding electronic waste.[7,11−17] However, these two material-based TTIs possess their own critical disadvantages, respectively. Chemical-reaction-based TTIs are usually activated at high-temperature ranges and thus are not applicable for vaccines that should be kept under subzero temperatures. In addition, the leakage and deactivation risks associated with these reactive additives remain a major concern.[7] The dye-diffusion-activated TTIs indicate time−temperature history *via* melting- and diffusing-induced color changes when exposed to temperatures above their melting points (T_m). Although these melting dye-diffusion-activated TTIs can operate at low temperatures, they still have significant drawbacks, including susceptibility to photobleaching, less temperature sensitivity, and narrow tracking temperature ranges. Therefore, new materials with high stability, sensitivity, and wide tracking temperature ranges are urgently needed for constructing reliable smart TTIs.

Structural color materials are emerging smart bioinspired materials with periodic structures, of which colors arise from the interactions between visible light and their periodical structures,[18] such as colloidal photonic crystals (PCs),[19−21] inverse opals,[22−25] cholesteric liquid crystals,[26,27] and Bragg wrinkles.[28,29] Among these smart structural color materials, responsive colloidal PCs have been intensively explored for displays, optical devices,[20,30] soft actuators,[22,24] and chemical-/biosensors,[21,23,31,32] owing to the easy availability of high-quality colloidal arrays and facile integration of stimuli-responsive functions.[33,34] Specifically, incorporating stimuli-responsive polymers or specific liquids into the voids of the colloidal PCs imparts dynamic tunability of structural color upon exposure to external stimuli, including chemicals,[21,24] mechanical force,[22,35,36] electric fields,[30,37−39] magnetic fields,[40−44] and thermal,[25,45] which induce changes in the refractive indices or/and the lattice constants of colloidal PCs. As one of the most important responsive colloidal PCs, thermal-responsive PCs can be created by introducing temperature-responsive hydrogels or shape memory polymers into the colloidal PCs, which can show rapid and brilliant color change when the temperature is increased above their lower critical solution temperatures or glass transition temperatures. But inevitably, the incorporation of responsive elements also brings unwanted issues.[25,45−52] First, the color changes triggered by the chain movements of thermal-responsive polymer-based PCs always occur at high temperatures (>0

https://doi.org/10.1021/acsnano.3c00467
ACS Nano 2023, 17, 10269−10279

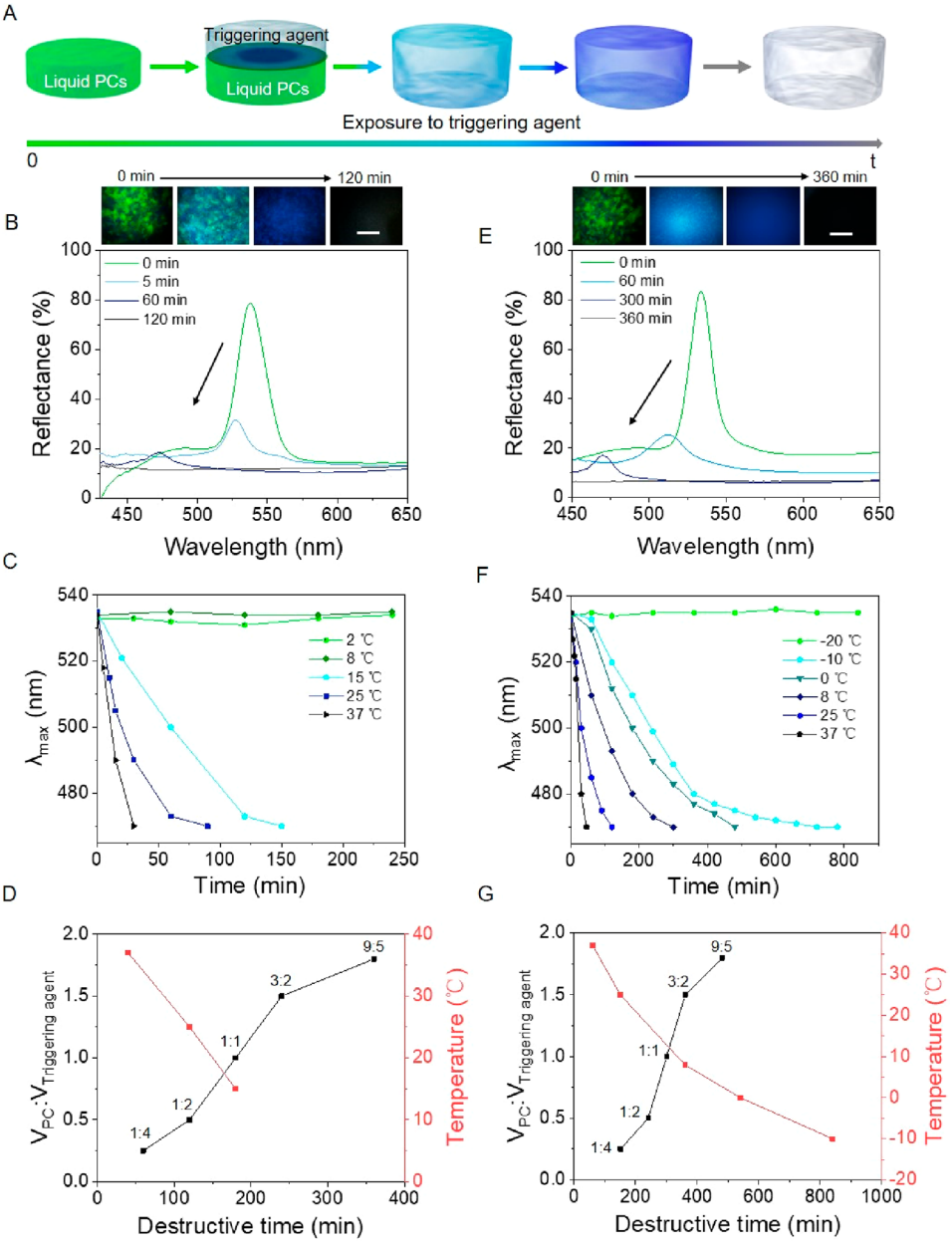

Figure 2. Programmable self-destruction. (A) Schematic illustration of the self-destructive behavior of the structural color liquid. (B) Variation of structural color and corresponding Bragg reflection of a self-destructive structural color liquid ($V_{PC}/V_{triggering\ agent}$ = 1:2; T_m of triggering agent: 8 °C) as exposure to 25 °C for 120 min. Scale bar: 500 μm. (C) Reflection variations of a self-destructive structural color liquid ($V_{PC}/V_{triggering\ agent}$ = 1:2; T_m of triggering agent: 8 °C) as exposure to different temperatures from 2 to 37 °C for different times. (D) Variation of destructive time *via* changing the $V_{PC}/V_{triggering\ agent}$ from 1:4 to 9:5 as exposure to 25 °C, and exposure temperature from 2 to 37 °C ($V_{PC}/V_{triggering\ agent}$ = 1:2; T_m of triggering agent: 8 °C), respectively. (E) Variation of structural color and corresponding Bragg reflection of a self-destructive structural color liquid ($V_{PC}/V_{triggering\ agent}$ = 3:2; T_m of triggering agent: −20 °C) as exposure to 8 °C for 360 min. Scale bar: 500 μm. (F) Reflection variations of a self-destructive structural color liquid ($V_{PC}/V_{triggering\ agent}$ = 3:2; T_m of triggering agent: −20 °C) as exposure to different temperatures from −20 to +37 °C for different times. (G) Variation of destructive time *via* changing the $V_{PC}/V_{triggering\ agent}$ from 1:4 to 9:5 (exposure to 8 °C) and exposure temperature from −10 to +37 °C ($V_{PC}/V_{triggering\ agent}$ = 3:2; T_m of triggering agent: −20 °C), respectively.

°C), implying poor temperature sensitivity and limited temperature range. Second, the existence of thermal-responsive elements also causes reversibility to recover their initial colors after removal of external stimuli. Therefore, developing thermal-responsive PCs with intrinsic structural color irreversibility and high sensitivity at low temperatures remains a big challenge, which limits their applications in cold-chain scenarios.

Here, we develop a class of structural color material, termed self-destructive structural color liquids, that harnesses advantages of both fluidic nature and structural color, imparting thermal-triggered visible color destruction based on triggering agent-diffusion-induced irreversible disassembly of liquid colloidal PCs for indicating the time−temperature history of the cold supply chain (Figure 1A). Different from conventional melting dye-diffusion-activated strategies, the self-destructive structural color liquids consist of two core units: (1) nontoxic

https://doi.org/10.1021/acsnano.3c00467
ACS Nano 2023, 17, 10269−10279

polyethylene glycol (PEG) or ethylene glycol (EG) aqueous solutions owing to their high sensitivity to specific temperatures and widely tunable T_m, termed as a triggering agent and (2) brilliant liquid colloidal PCs owing to its fluidic nature and nonphotobleaching structural color, termed as an indicating agent (Figure 1B,C). Leveraging on the synergy of these two units, the self-destructive structural color liquids possess an excellent capability of indicating time−temperature history, including notable irreversible color change, superior sensitivity, largely tunable self-destructive time (40 min∼5 days), and a wide tracking temperature range from −70 to +37 °C. Due to the inherent fluidic nature of both triggering agents and indicating agents, such self-destructive structural color liquids can be facilely packaged into flexible liquid colloidal photonic crystal-based TTIs (P-TTIs) with diverse forms (*e.g.*, round labels, QR codes). More importantly, we further extend these P-TTIs to monitoring diverse products of the cold supply chain, ranging from conventional vaccines (storage temperature: 8 °C), mRNA vaccines (storage temperature: −20 and −70 °C) to the transported organ (storage temperature: 0 °C). Our self-destructive structural color liquids overcome the disadvantages inherent in conventional TTIs and responsive PCs, bringing them one step close to the cold supply chain, and hold promise for the next-generation intelligent TTIs and PCs.

RESULTS AND DISCUSSION

Fabrication of Self-Destructive Structural Color Liquids. To fabricate self-destructive structural color liquids, we first prepared the temperature-sensitive triggering agents and tuned their T_ms. Typically, PEG and EG aqueous solutions were chosen as the triggering agents, aiming to impart tunable T_m and strong molecular interaction with the following indicating agents. According to the well-known solution theory, a series of triggering agents with on-demand melting temperatures (*e.g.*, −70, −20, and +8 °C) can be customized by facilely varying the ratio of PEG/water and EG/water, respectively (Figure S1). These triggering agents can be facilely frozen and kept in solid states ($T < T_m$) and then melted into liquid states as exposed to a temperature above their corresponding T_m, enabling high sensitivity to a specific temperature.

Second, we prepared the structural color indicating agent, that is, liquid colloidal PCs (*i.e.*, microcrystal arrays dispersed in glycerol), by concentrating colloidal suspension above a critical concentration (Figure S2). Briefly, monodisperse SiO_2 particles were synthesized by the Stöber method[53] and then washed, concentrated, and finally self-assembled in nontoxic and recyclable glycerol (see the Materials and Methods section). Different from traditional responsive PCs and dyes, liquid colloidal PCs exhibit fluidic nature and nonphotobleaching structural color. Figure 1D shows that the liquid colloidal PCs contain numerous glycerol-wrapped microsized colloidal microcrystal arrays, which are stabilized by the synergistic interaction of van der Waals attraction and electrostatic repulsion of neighboring SiO_2 particles within the microcrystal arrays.[54,55] Such microcrystal arrays can maintain stable periodic structures not only over a wide temperature range from −70 to +25 °C but also for several months at room temperature (Figure 1D and Figure S3). Notably, this outstanding stability of liquid colloidal PCs at a wide temperature range attributed to the rational choice of glycerol with a high boiling point and high viscosity, which inhibit the Brownian motion-induced disassembly of colloidal crystals. Furthermore, the abundant hydroxyl (OH) groups in glycerol also endow robust moisture absorption of the liquid colloidal PCs. As shown in Figure S4, the liquid colloidal PCs appear colorless at a very low relative humidity of 40 RH%. Increasing the relative humidity from 40 to 70 RH%, the liquid colloidal PCs exhibit colorless, blue, blue-green, and brilliant green colors, respectively, because the absorbed small amount of water molecules enhances the interaction of negatively charged SiO_2 particles and facilitates their assembly, which provides a universal strategy for assembling particles in a high-viscosity solvent, which is deemed impossible in the previous work.[55] Under an appropriate humidity (∼70 RH%), the liquid colloidal PCs display uniform and bright structural color, attributing to the strong coherent diffraction of visible light in the nonclose-packed colloidal crystal arrays as revealed by optical microscopic and scanning electron microscopy (SEM) images (Figure 1D). Notably, these glycerol-wrapped nonclose-packed colloidal crystal arrays are highly sensitive to glycerol variation (Figure S5). By increasing the glycerol concentration (*i.e.*, decreasing the particle concentration from 69 to 51 to 27 wt %), the structural color of liquid colloidal PCs shifts from green to red and finally to colorless owing to the increased interparticle distance (Figure 1E). In addition, the liquid colloidal PCs can be facilely cast into various brilliant patterns (Figure 1F,G and Figure S6), such as "IBMD" letters with various colors, and a QR code filled with both frozen triggering agent and liquid colloidal PCs.

Self-Destructive Behaviors. We next investigate the self-destructive behaviors of the combined system composed of both highly temperature-sensitive triggering agents and solvent-sensitive liquid colloidal PCs. When exposed to a certain temperature ($T > T_m$ of triggering agent), the triggering agent flows to the liquid colloidal PCs, causing noticeable time-related color change owing to the irreversible solution mixing of the combined system (Figure 2A). Figure S7 shows that the self-destructive structural color liquid (T_m: 8 °C, $V_{PC}/V_{triggering\ agent}$ = 1:2) can be stably stored at a temperature range of 2−8 °C and exhibits brilliant green color. As exposed to a temperature of 25 °C, the structural color of the self-destructive structural color liquid turns blue within 5 min and gradually decays to colorless in 120 min (Figure 2B). Increasing the exposure temperature from 25 to 37 °C leads to a faster color change of the self-destructive structural color liquid, thus shortening the destructive time from 120 to 40 min (Figure 2C,D and Figure S7). Such results suggest the self-destructive progress is highly dependent on the exposure time and temperature of the self-destructive structural color liquid because the mixing degree between the PEG aqueous solution and the liquid colloidal PCs increases with extending the exposure time or increasing the exposure temperature, based on diffusion kinetics. Notably, the destructive time of the self-destructive structural color liquids can be tailored by tuning the volume ratio of the liquid colloidal PCs and the triggering agent ($V_{PC}/V_{triggering\ agent}$). Figure 2D and Figure S8 show that decreasing the volume ratio of the PEG aqueous solution from 1:4 to 9:5 extends the self-destructive time from 60 to 360 min. It is worth noting that not only the tracking temperature of the self-destructive structural color liquids can even be facilely programmed to subzero (−20 and −70 °C) but also the self-destructive time can be extended to days by tuning both T_m, volume ratio, or the molecular weight of the triggering agent, thus meeting the time−temperature indicating requirements of

https://doi.org/10.1021/acsnano.3c00467
ACS Nano 2023, 17, 10269−10279

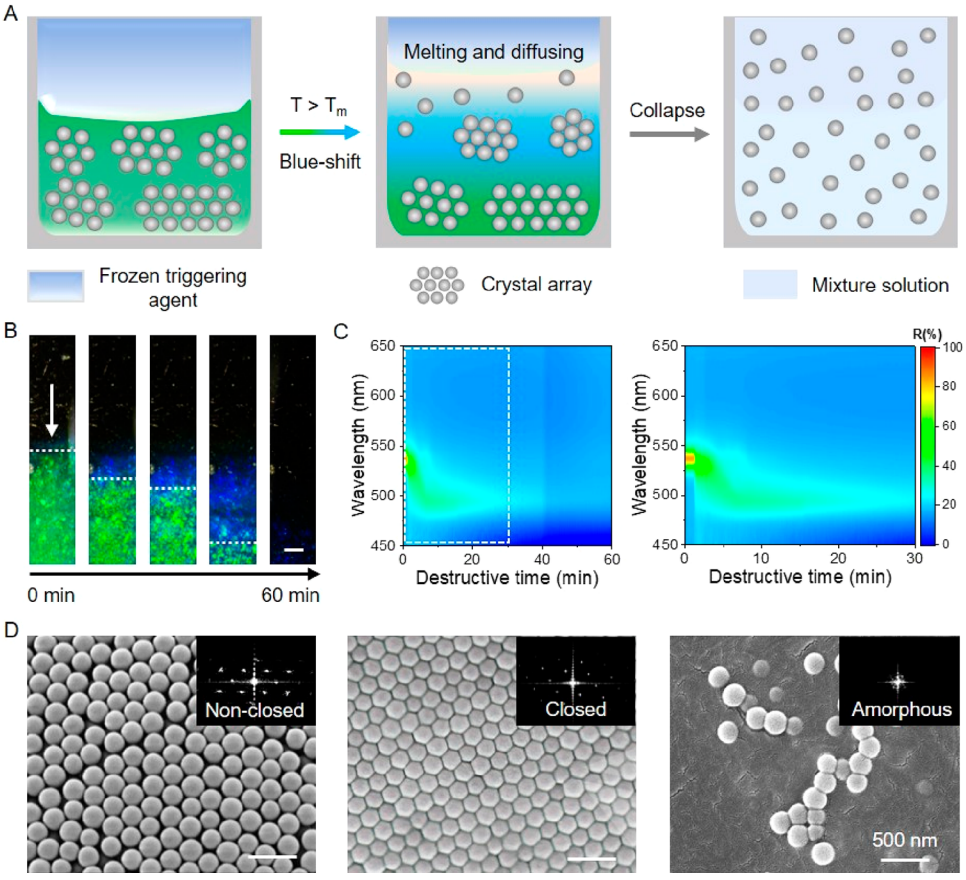

Figure 3. Self-destructive mechanism. (A) Schematic illustration of the abuse temperature-induced melting and diffusing of triggering agent, finally leading to collapse of the microcrystal arrays. (B) Interface color change by exposing liquid colloidal PCs to PEG aqueous solution. Scale bar: 200 μm. (C) Dynamic reflectance spectra of the self-destructive progress and enlarged dynamic reflectance spectra in the early 30 min. (D) SEM and the inserted fast Fourier transformation images show the periodic structure variations of the colloidal crystal arrays at the interface, corresponding with bright green color (left, nonclosed crystal array), blue color (middle, closed crystal array), and colorless (right, amorphous structures), respectively. The SEM images share the same scale bar.

both conventional and mRNA vaccines (Figure 2E−G and Figures S9−S12).[4] Such results suggest the self-destructive structural color liquids exhibit inherent irreversibility, noticeable color change, tunable self-destructive time, and programmable tracking temperature. Theoretically, the self-destructive time and temperature can be customized to meet the specific requirements of various temperature-sensitive products.

Self-Destructive Mechanism. We then reveal the self-destructive mechanism of structural color liquids. As schemed in Figure 3A, the frozen triggering agent in the top layer begins to melt when exposed to a temperature higher than its T_m. The molecules of the melted triggering agent then interact with glycerol molecules in the liquid colloidal PCs in the bottom layer, thus disturbing the periodic structures of colloidal crystal arrays at the interface. Correspondingly, the liquid colloidal PCs change color and finally turn colorless. Such triggering agent melting-to-diffusing induced periodical structure changes can be described by Bragg's law. The maximum characteristic reflection peak quantifying the periodic structures can be expressed *via* the following equation:

$$\lambda_{max} = 1.633\frac{D}{m}\sqrt{\sum n_i^2\phi_i - \sin^2\theta}$$

where λ_{max} is the reflection wavelength, D is the interparticle distance, m is the diffraction order, n_i and ϕ_i are the refractive index and volume fraction of the suspension, and θ is the angle between the sample normal and incident light.[56] Theoretically, D, n_i, and ϕ_i would change as the triggering agent mixes with the liquid colloidal PCs, resulting in the final structural color change of the liquid colloidal PCs.

Consistent with the above theoretical analysis, our experiments demonstrate that the structural color of the liquid colloidal PCs is closely related to the particle concentration and interparticle distance. As shown in Figure 3B, the initial interface exhibits brilliant green color of the liquid colloidal PCs owing to the transparency of the PEG aqueous solution. Rapidly, the green interface turns into blue color and then becomes transparent. Such color transformation finally spreads to the whole liquid colloidal PCs within 60 min, attributing to both solvent diffusion and Brownian motion of colloidal particles at the interface (Movie S1). Specifically, owing to the difficult mobility of the water-bound PEG 1000,[57] the PEG 1000 aqueous solution extracts glycerol molecules from the liquid colloidal PCs, leading to an increase in the particle concentration, thus decreasing the interparticle distance and causing instability of the glycerol-wrapped colloidal crystal arrays on one hand.[58] On the other hand, the extracted glycerol molecules break the binding of water molecules and PEG chains, and these released molecules then disturb the metastable crystal arrays at the interface, leading to significantly increased Brownian motion of the SiO_2 nanoparticles and the final collapse of crystal arrays. Interestingly,

https://doi.org/10.1021/acsnano.3c00467
ACS Nano 2023, 17, 10269−10279

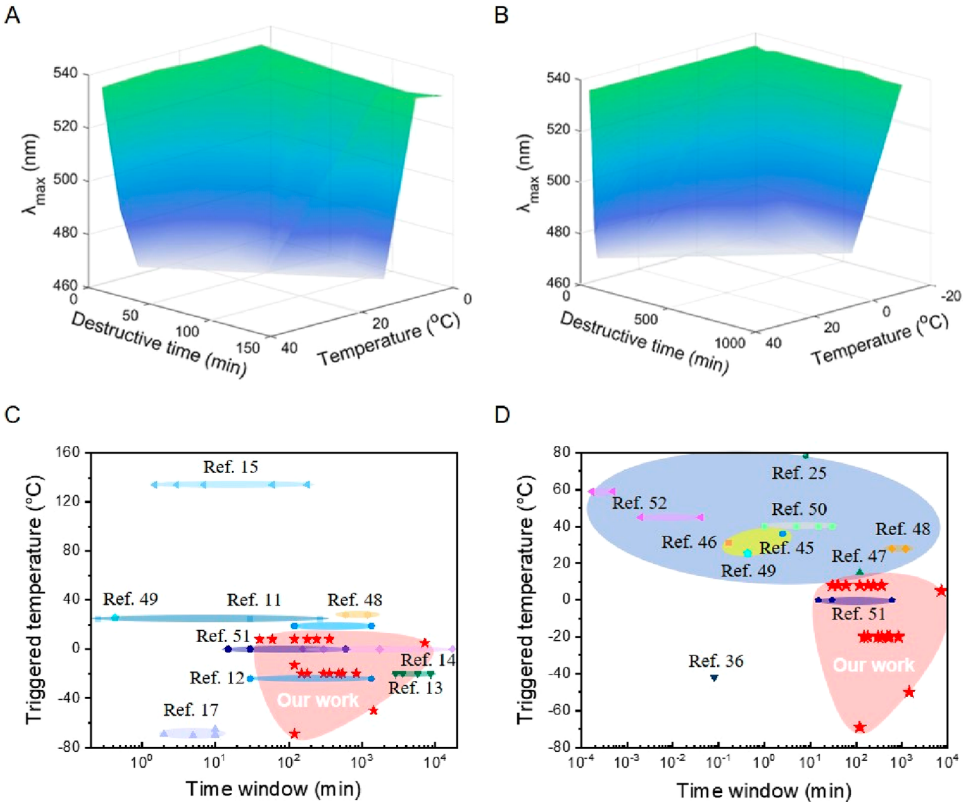

Figure 4. Advantages of the self-destructive structural color liquids. (A and B) λ_{max}−time−temperature relationship of the self-destructive structural color liquids with T_m of +8 and −20 °C, indicating the tunable destructive time and programmable tracking temperature. (C) Comparisons of the time window and triggered temperature with previous materials-based TTIs. (D) Comparisons of time window and triggered temperature with previous temperature-responsive structural color materials (blue region, polymer-based temperature-responsive structural color materials; yellow region, reversible polymer-based temperature-responsive structural color materials).

using PEG 600 solely as the triggering agent leads to a similar green-to-blue transformation of the liquid colloidal PCs, and the final blue color can remain for more than 21 days without collapse, indicating the formation of new metastable crystal arrays. By contrast, owing to the high viscosity feature of glycerol, small molecule-based triggering agents (*e.g.*, water, EG aqueous solution, EG, PEG 200, and PEG 400) diffuse into glycerol (Figures S12 and S13), leading to a decrease in the particle concentration, an increase in the interparticle distance, and thus the green-to-red transformation and final collapse of the crystal arrays.[24,59] Such solvent diffusion disturbs the balance between the van der Waals attraction and electrostatic repulsion of neighboring negatively charged SiO_2 nanoparticles,[54,60] causing irreversible transformation and collapse of the colloidal crystal arrays that can be evidenced by dynamic reflectance spectra, SEM, and fast Fourier transformation images (Figure 3C,D). Notably, using pure EG or PEG as the triggering agent or increasing the molecule weight of the triggering agent (*e.g.*, EG, PEG 200, to PEG 400) decreases the molecule mobility, both of which will extend the diffusion-induced final destruction time to days (Figure S12).

Notably, the triggering agent diffusion-induced structural color destruction can be further revealed by the λ_{max}-time−temperature relationship, which demonstrates that the self-destruction progresses within a shorter time as exposure to a higher temperature based on diffusion kinetics and Brownian motion (Figure 4A,B). Compared to previous material-based TTIs[11−17,61] and temperature-responsive structural color materials,[25,36,45−52] our structural color liquids for visibly indicating time−temperature history demonstrate outstanding overall performances in inherent irreversibility, high sensitivity, tunable self-destructive time (40 min ∼ 5 days), and wide tracking temperature range (−70 ∼ +37 °C) even at low temperatures (Figure 4C,D), which are critical for indicating the time−temperature history of vaccines yet is impossible for conventional TTIs (Tables S1 and S2).

Applications of self-destructive structural color liquids. The big challenge hindering the practical applications of current TTIs for indicating the time−temperature history of vaccines is the limited reliability and stability owing to their inapplicability for subzero temperatures, narrow tracking temperature ranges, and poor sensitivity. Leveraging on the distinctive advantages, we harness the self-destructive structural color liquids to indicate the time−temperature history of diverse cold-chain scenarios. Owing to the fluidic nature and stable structural color (Movie S2), the triggering agent and liquid colloidal PCs can be facilely integrated into a closed system, that is P-TTI (Figures S14 and S15). As shown in Figure 5A, the P-TTI can be facilely prepared by filling the triggering agent and liquid colloidal PCs into the outer and inner rings of the round CNT@PDMS label, respectively, followed by sealing with a transparent PDMS film (see the Materials and Methods section). Three types of P-TTIs (storage temperature: +8, −20, and −70 °C) were adhered to vaccine vial prototypes for indicating the status of normal and mRNA COVID-19 vaccines, respectively. Such P-TTIs can be stably stored at the recommended temperatures (+8, −20, and −70 °C) of the WHO for more than 2 weeks without apparent

https://doi.org/10.1021/acsnano.3c00467
ACS Nano 2023, 17, 10269−10279

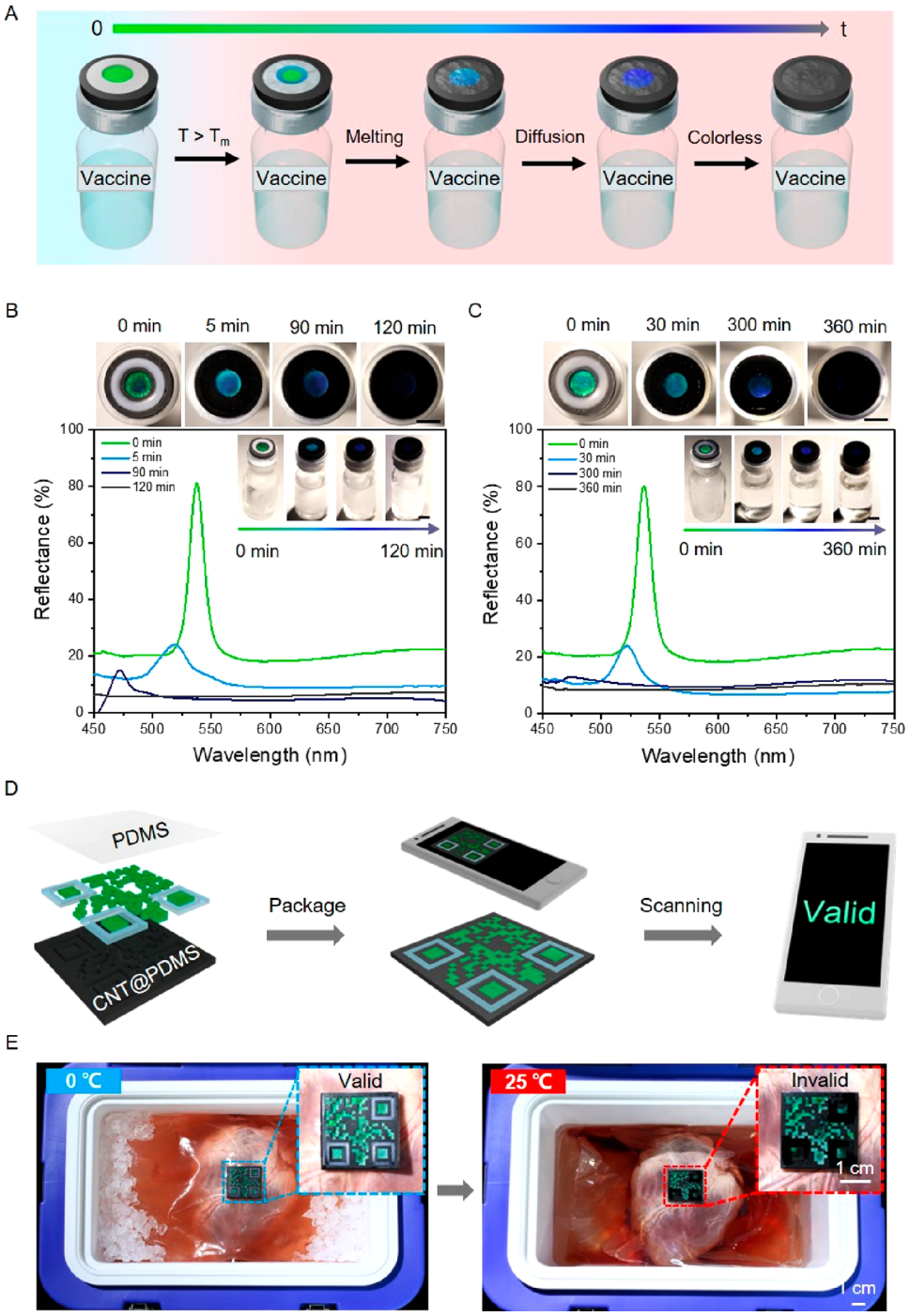

Figure 5. Time−temperature indicating applications. (A) Schematic illustration of the triggering agent melting-to-diffusing induced destruction of a P-TTI for indicating the time−temperature history of a vaccine. (B) Optical photographs and reflectance spectra of a P-TTI for monitoring the storage status (8 °C) and exposure to 25 °C for 120 min. Scale bar: 5 mm. (C) Optical photographs and reflectance spectra of a P-TTI for monitoring the storage status (−20 °C) and exposure to 8 °C for 360 min. Scale bar: 5 mm. (D) Schematically illustrating the structure of a P-TTI with a QR code that can be scanned *via* a mobile phone. (E) Optical photographs of a porcine heart with an intact QR code stored in an ice box (0 °C) and a destructive QR code as exposed to an abuse temperature (25 °C) for 360 min.

color change (Figures S11 and S16). As exposure to 25 °C for 120 min, the P-TTI (8 °C) showed noticeable color change (Figure 5B), which meets the strict requirements of time−temperature history of the WHO recommendation for the normal vaccine, Oxford-AstraZeneca.[62] Furthermore, the P-TTI (−20 °C) can be used for monitoring the status of mRNA vaccine. Specifically, the P-TTI with initial brilliant green color turns colorless when exposed to 8 °C for 360 min (Figure 5C), which corresponds to the use requirements of Moderna according to WHO recommendation.[62] Similarly, the P-TTI (−70 °C) with initial red color showed the noticeable color change upon exposure to −20 °C for 60 min, which can be used for monitoring the status of Pfizer-BioNTech (Figure S17). Notably, the gradual color changes and reflectance spectra shift provide a synergistic strategy for qualitatively and quantitatively revealing the accurate time−temperature history

https://doi.org/10.1021/acsnano.3c00467
ACS Nano 2023, 17, 10269−10279

of various vaccines. Such results suggest that our P-TTIs not only possess superior high stability at the recommended storage temperature for a long time but also can be used for vividly indicating the time−temperature history with high sensitivity for both normal and mRNA vaccines. Moreover, the exposure status of a P-TTI can be clearly recorded even after being refrozen or remelted (Figure S18).

Aside from indicating the status of diverse vaccines, the P-TTI can also be customized into a QR code for monitoring the temperature history of an isolated organ, which plays a vital role in organ transplantation.[63] To demonstrate high sensitivity to nonuniform thermal alteration, the triggering units are located at three separate sites of the QR code. Figure 5D shows that a P-TTI adheres to a plastic bag with a porcine heart, which is stored in a specific box with an ice bath to mimic the transported organ storage. Normally, the QR code information on "valid" in the P-TTI can be facilely scanned *via* a mobile phone, suggesting nonexposure to ambient temperature. However, the QR code information would finally lose after the organ exposure to 25 °C for 6 h owing to the thermal-triggered destruction of the QR code, indicating the "invalid" status of the transported organ (Figure 5E). Such P-TTI containing both color and digital information not only avoids human intervention but also provides great convenience for users. Incorporating 3D-printing technology, various P-TTI with diverse digital information can realize low-cost mass production.

CONCLUSION

In summary, we developed a distinctive strategy for indicating time−temperature history that harnesses the distinctive advantages of self-destructive structural color liquids, which comprise a triggering agent and liquid colloidal PCs. We demonstrate that the self-destructive structural color liquids impart a wide tracking temperature range due to the facilely tunable melting point of triggering agents (−70 ∼ +8 °C). Leveraging on its fluidic nature, we also show that the self-destructive structural color liquids eliminate the inherent reversibility, low sensitivity, and narrow tracking temperature in conventional temperature-responsive PCs at low temperatures. Compared with previous TTIs, our strategy endows high flexibility and superior reliability in time−temperature indicating, including outstanding stability (4 months), high sensitivity, wide tracking temperature range (−70 ∼ +37 °C), and largely tunable time window (minutes ∼ days). Outperforming existing methods in terms of tracking temperature range, sensitivity, and user-friendly, self-destructive structural color liquids with thermally triggered destruction capabilities have established a general design rule for next-generation intelligent indicators, holding promise for reliable cold chains. In addition, we anticipate that structural color liquids will benefit various areas such as wearable sensors, droplet robots, and photonic display.[37,64−67]

MATERIALS AND METHODS

Materials. Glycerol (99%), polyethylene glycol (PEG 200, 400, 600, and 1000, M_w: 200, 400, 600, and 1000), and aqueous ammonia (28%) were purchased from Sigma-Aldrich. Ethanol (99.9%) and ethylene glycol (EG, 99.5%) were purchased from Sinopharm Chemical Reagent Co., Ltd. (Shanghai, China). Tetraethyl orthosilicate (TEOS, ≥ 99.9%) was purchased from Aladdin Biochemical Technology (Shanghai, China). Polydimethylsiloxane (PDMS, Sylgard 184 silicone elastomer kit) was purchased from Dow Corning Co., Ltd. (Midland, MI). Multiple-wall carbon nanotubes (CNTs, average length: 20 μm) were purchased from Xianfeng Nano Co., Ltd. (Nanjing, China). Isolated porcine heart was purchased from the local market (Shenzhen, China). Ultrapure water (18.2 MΩ·cm) was produced by a water purification system (Arioso Power II, Human, Korea) and used throughout this study.

Fabrication of PDMS Molds. PDMS molds of diverse types (cylinder labels, inner diameter × depth = 2.5 mm × 2.5 mm; "IBMD" pattern, 5 mm length and 1.5 mm height for each letter; QR-code labels, length × width × height = 25 mm × 25 mm × 1.5 mm, length × width × depth = 1 mm × 1 mm × 0.95 mm for each pixel; round labels with an outer ring and an inner ring at different depths, outer ring diameter × depth = 13 mm × 1 mm, inner ring diameter × depth = 5 mm × 2 mm; and slope angle of the outer ring, ∼ 12°) were fabricated by filling precursor mixtures (curing agent/prepolymer = 1:10 (w/w), 1 wt % CNTs) into the predesigned poly(methyl methacrylate) (PMMA) or resin molds and then cured at 70 °C for 2 h. Afterward, the black CNT@PDMS molds were then peeled off from the PMMA or resin molds for the following experiments. Noting that the addition of CNTs is to enhance the color contrast of the subsequently added liquid colloidal PCs.

Preparation of Triggering Agents. The triggering agents with various T_ms were prepared by mixing PEG 1000 or EG with water in appropriate ratios (Figure S1).[17] Typically, triggering agents with melting points of −70, −20, and +8 °C were obtained by preparing EG/water (70.0 wt %), PEG 1000/water (64.5 wt %), and PEG 1000/water (69.0 wt %) solutions, respectively, which were used for the following experiments. In addition, pure EG, PEG 200, PEG 400, and PEG 600 were also used as the triggering agent, respectively.

Preparation of Liquid Colloidal PCs. Monodispersed SiO_2 particles with various sizes (173, 190, 202, and 235 nm) were synthesized by the classical Stöber method.[53] The as-synthesized particles were purified by centrifugal washing in water and ethanol (at least 3 times for each), respectively. Then, the colloidal suspension (25 wt % in ethanol) was mixed with a predetermined weight of glycerol. Consequently, the colloidal suspension with various solid contents (27, 43, 47, 51, 60, and 69 wt %) were obtained after evaporating ethanol at 50 °C for 12 h. Finally, the liquid colloidal PCs with bright structural colors were prepared after assembling at 25 °C for 24 h (70 RH%). For example, the brilliant "IBMD" letters were prepared by filling the colloidal suspension (10 μL for each letter) with different particle sizes (I, 173 nm; B, 190 nm; M, 235 nm; D, 202 nm) into the former PDMS mold at 25 °C for 24 h (70 RH%).

To assess the temperature stability, 69 wt % liquid colloidal PCs (particle size: 235 and 190 nm) were added into the former cylinder PDMS molds, then sealed with 100-μm-thick transparent PDMS films, and finally exposed to various environmental temperatures (−70, −20, +8, +25, and +37 °C) for 24 h. In addition, 69 wt % liquid colloidal PCs (particle size: 190 nm) were exposed to different environmental humidity (40, 50, 60, 70, and 80 RH%) at 25 °C for 1 h to investigate the humidity sensitivity. Thus, the following labels were sealed with 100-μm-thick transparent PDMS films to avoid humidity disturbance.

Unless specifically mentioned, the liquid colloidal PCs (69 wt %) were assembled at 25 °C for 24 h for the following experiments (70 RH%).

***In Situ* Monitoring of Destructive Behaviors of the Structural Color Liquids (SCLs).** The self-destructive SCLs consist of two units, including the triggering agent and indicating agent (*i.e.*, the liquid colloidal PCs). First, self-destructive SCLs with different triggering agents (T_m: +8 and −20 °C) and various $V_{PC}/V_{triggering\ agent}$ values (1:4, 1:2, 1:1, 3:2, and 9:5; V_{PC}: 3 μL) were exposed to an environmental temperature of 25 °C to reveal the relationship between the $V_{PC}/V_{triggering\ agent}$ and the self-destructive time, respectively. Second, self-destructive SCLs with a certain triggering agent (69.0 wt % PEG 1000/water solution, T_m: 8 °C) and $V_{PC}/V_{triggering\ agent}$ = 1:2 (V_{PC}: 3 μL, 69 wt %) were exposed to 2, 8, 15, 25, and 37 °C to study the relationship between the exposed temperature and the self-destructive time. In addition, self-destructive SCLs with a certain triggering agent (64.5 wt % PEG 1000/water solution, T_m:

https://doi.org/10.1021/acsnano.3c00467
ACS Nano 2023, 17, 10269−10279

−20 °C) and $V_{PC}/V_{triggering\ agent}$ = 3:2 (V_{PC}: 3 μL, 69 wt %) were exposed to −20, −10, 0, +8, +25, and +37 °C to study the relationship between the abuse temperature and self-destructive time. Furthermore, the self-destructive dynamics of the self-destructive SCLs have also been investigated. Specifically, 3 μL of suspension of liquid colloidal PCs (69 wt %) was added into the channel of a PDMS mold (length × width × depth = 10 mm × 2 mm × 1 mm) first. Then, 40 μL of triggering agent (64.5 wt % PEG 1000/water solution, T_m: −20 °C) was added to the other side of the channel. As the triggering agent flowed into the liquid colloidal PCs, the color of the liquid−liquid interface finally changed.

Self-Destructive SCLs for Indicating Time−Temperature History. P-TTIs were prepared by adding 10 μL liquid colloidal PCs (particle size: 190 nm, 69 wt %) into the inner ring of the round labels and then assembled at 25 °C for 7 days. Afterward, 30 μL triggering agents with different T_m values (−20 °C for 64.5 wt % PEG 1000/water solution; 8 °C for 69.0 wt % PEG 1000/water solution) were then added into the outer ring of the round labels, respectively. The sealed P-TTIs (T_m of triggering agent: −20 and +8 °C) were obtained after freezing the triggering agents into solid states by using dry ice as a cooling agent. Similarly, the P-TTIs with a T_m of −70 °C (70.0 wt % EG/water solution) were also prepared as mentioned above. These P-TTIs (T_m of triggering agent: −70, −20, and +8 °C) adhered onto vaccine vial prototypes (filled with 1.5 mL water) were then exposed to −20, +8, and +25 °C, correspondingly. Note that the triggering agent is not in direct contact with liquid colloidal PCs to ensure structural color stability of the P-TTI *via* a rational design of the round CNT@PDMS label. Specifically, the design of the outer ring and inner ring at different depths of the label avoids the direct contact of the triggering agent and liquid colloidal PCs. The slope angle of the outer ring assistants the flowing of melted triggering agent into the liquid colloidal PCs by gravity.

For QR-code P-TTI, 150 μL of liquid colloidal PCs (particle size: 190 nm) was added into the data area, and then assembled at 25 °C for 14 days. Subsequently, 30 μL of triggering agent (69.0 wt % PEG 1000/water solution, T_m: 8 °C) was added into each of the three position detection patterns. Finally, the sealed QR-code P-TTI was frozen in a −20 °C refrigerator for 30 min. For monitoring the time−temperature information on an isolated porcine heart, the QR-code P-TTI was adhered onto a plastic bag with a porcine heart, which is stored in a specific box with an ice bath to mimic the transported organ storage.

Characterization. The colloidal assemblies' images were recorded by a field-emission scanning electron microscope (SEM, Sigma 300, Carl Zeiss) after a freeze-drying process for 24 h. The digital photographs were captured by a digital camera (Canon EOS 6D Mark II). The *in situ* reflection spectra were measured by a fiber optical spectrometer (HR 2000+, Ocean Optics) that was coupled with an optical microscope (Ni−U, Nikon). The microscopic optical images were captured by an optical microscope (dark field mode, Olympus GX 51). The interface color changes at the triggering agent and the liquid colloidal PCs were recorded by a stereo microscope (SZ 69, Olympus). A homemade hot bench was used to provide a specific temperature of 37 °C. The λ_{max}−time−temperature relationship of the self-destructive SCLs were calculated using MATLAB.

ASSOCIATED CONTENT

Supporting Information

The Supporting Information is available free of charge at https://pubs.acs.org/doi/10.1021/acsnano.3c00467.

Figures of properties of trigger agent, assembly of SCLs, stability, humidity, and solvent sensitivity of SCLs, SCLs with various sizes of SiO_2, self-destructive behaviors of a self-destructive SCL, different temperature and time windows of SCLs, interface color change of SCLs, pressure sensitivity of SCLs, optical photographs and reflectance spectra of a P-TTI, and refreezing properties of P-TTIs and tables of temperature and time windows comparison of SCLs with reported TTIs and comparison of our liquid colloidal PCs strategy (PDF)

Movie of interface color change *via* exposing liquid colloidal PCs to PEG 1000 aqueous solution (MP4)

Movie of color change of liquid colloidal PCs upon and after exposure to top gas blowing (MP4)

AUTHOR INFORMATION

Corresponding Authors

Yadong Yin − *Department of Chemistry, University of California Riverside, Riverside, California 92521, United States;* orcid.org/0000-0003-0218-3042; Email: yadong.yin@ucr.edu

Xuemin Du − *Institute of Biomedical & Health Engineering, Shenzhen Institute of Advanced Technology (SIAT), Chinese Academy of Sciences (CAS), Shenzhen 518055, P. R. China;* orcid.org/0000-0002-0200-5759; Email: xm.du@siat.ac.cn

Authors

Chao Huang − *Institute of Biomedical & Health Engineering, Shenzhen Institute of Advanced Technology (SIAT), Chinese Academy of Sciences (CAS), Shenzhen 518055, P. R. China*

Yuanyuan Shang − *Institute of Biomedical & Health Engineering, Shenzhen Institute of Advanced Technology (SIAT), Chinese Academy of Sciences (CAS), Shenzhen 518055, P. R. China; School of Chemistry and Chemical Engineering, Guangxi University, Nanning 530004, P. R. China*

Jiachuan Hua − *Institute of Biomedical & Health Engineering, Shenzhen Institute of Advanced Technology (SIAT), Chinese Academy of Sciences (CAS), Shenzhen 518055, P. R. China*

Complete contact information is available at: https://pubs.acs.org/10.1021/acsnano.3c00467

Author Contributions

X.D. conceived the idea and research. X.D. and C.H. designed the experiments. C.H. conducted the experiments with assistance of Y.S. and J.H. X.D. supervised the study, analyzed the results, and wrote the manuscript. Y.Y. revised the manuscript. All authors contributed to the discussion and interpretation of the results.

Notes

The authors declare no competing financial interest.

ACKNOWLEDGMENTS

The authors acknowledge the financial support provided by National Natural Science Foundation of China (52022102, 52261160380), National Key R&D Program of China (2017YFA0701303), the Youth Innovation Promotion Association of CAS (2019353), Guangdong Regional Joint Fund-Key Project (2021B1515120076), CAS Key Laboratory of Health Informatics, Shenzhen Institutes of Advanced Technology (2011DP173015), and the Fundamental Research Program of Shenzhen (RCJC20221008092729033, JCYJ20220818101800001). The authors thank Prof. Le He from Soochow University for inspiring discussions.

REFERENCES

(1) *COVID-19 Weekly Epidemiological Update*, ed 115; World Health Organization, 19 October 2022.

(2) Hanson, C. M.; George, A. M.; Sawadogo, A.; Schreiber, B. Is Freezing in the Vaccine Cold Chain an Ongoing Issue? A Literature Review. *Vaccine* **2017**, *35*, 2127−2133.
(3) Matthias, D. M.; Robertson, J.; Garrison, M. M.; Newland, S.; Nelson, C. Freezing Temperatures in the Vaccine Cold Chain: a Systematic Literature Review. *Vaccine* **2007**, *25*, 3980−3986.
(4) Fahrni, M. L.; Ismail, I. A.-N.; Refi, D. M.; Almeman, A.; Yaakob, N. C.; Saman, K. M.; Mansor, N. F.; Noordin, N.; Babar, Z.-U.-D. Management of COVID-19 Vaccines Cold Chain Logistics: a Scoping Review. *J. Pharm. Policy Pract.* **2022**, *15*, 16.
(5) Holm, M. R.; Poland, G. A. Critical Aspects of Packaging, Storage, Preparation, and Administration of mRNA and Adenovirus-Vectored COVID-19 Vaccines for Optimal Efficacy. *Vaccine* **2021**, *39*, 457−459.
(6) Ramakanth, D.; Singh, S.; Maji, P. K.; Lee, Y. S.; Gaikwad, K. K. Advanced Packaging for Distribution and Storage of COVID-19 Vaccines: a Review. *Environ. Chem. Lett.* **2021**, *19*, 3597−3608.
(7) Weston, M.; Geng, S.; Chandrawati, R. Food Sensors: Challenges and Opportunities. *Adv. Mater. Technol.* **2021**, *6*, 2001242.
(8) Wang, S.; Liu, X.; Yang, M.; Zhang, Y.; Xiang, K.; Tang, R. Review of Time Temperature Indicators as Quality Monitors in Food Packaging. *Packaging Technology and Science* **2015**, *28*, 839−867.
(9) Allegra, J. R.; Baughman, R. H. Vaccine Time-Temperature Indicators for Present and Future viral Threats. *Vaccine* **2020**, *38*, 6967−6968.
(10) Tao, H.; Brenckle, M. A.; Yang, M.; Zhang, J.; Liu, M.; Siebert, S. M.; Averitt, R. D.; Mannoor, M. S.; McAlpine, M. C.; Rogers, J. A.; et al. Silk-Based Conformal, Adhesive, Edible Food Sensors. *Adv. Mater.* **2012**, *24*, 1067−1072.
(11) Romano, L.; Portone, A.; Coltelli, M.-B.; Patti, F.; Saija, R.; Iatì, M. A.; Gallone, G.; Lazzeri, A.; Danti, S.; Maragò, O. M.; Camposeo, A.; Pisignano, D.; Persano, L. Intelligent Non-Colorimetric Indicators for the Perishable Supply Chain by Non-Wovens with Photo-Programmed Thermal Response. *Nat. Commu.* **2020**, *11*, 5991.
(12) Choi, S.; Eom, Y.; Kim, S.-M.; Jeong, D.-W.; Han, J.; Koo, J. M.; Hwang, S. Y.; Park, J.; Oh, D. X. A Self-Healing Nanofiber-Based Self-Responsive Time-Temperature Indicator for Securing a Cold-Supply Chain. *Adv. Mater.* **2020**, *32*, 1907064.
(13) Chen, Y.; Song, Y.; Zhang, Z.; Chen, Y.; Deng, Q.; Wang, S. Thiol-Functionalized Covalent Organic Frameworks As Thermal History Indictor for Temperature and Time History Monitoring. *Adv. Funct. Mater.* **2021**, *31*, 2104885.
(14) Zhang, C.; Yin, A.-X.; Jiang, R.; Rong, J.; Dong, L.; Zhao, T.; Sun, L.-D.; Wang, J.; Chen, X.; Yan, C.-H. Time-Temperature Indicator for Perishable Products Based on Kinetically Programmable Ag Overgrowth on Au Nanorods. *ACS Nano* **2013**, *7*, 4561−4568.
(15) Lee, B. S.; Shin, H. S. Polymer-Based Time-Temperature Indicator for High Temperature Processed Food Products. *Food Sci. Biotechnol.* **2012**, *21*, 1483−1487.
(16) Yousefi, H.; Ali, M. M.; Su, H. M.; Filipe, C. D. M.; Didar, T. F. Sentinel Wraps:Real-Time Monitoring of Food Contamination by Printing DNAzyme Probes on Food Packaging. *ACS Nano* **2018**, *12*, 3287−3294.
(17) Hao, L. T.; Lee, M.; Jeon, H.; Koo, J. M.; Hwang, S. Y.; Oh, D. X.; Park, J. Tamper-Proof Time-Temperature Indicator for Inspecting Ultracold Supply Chain. *ACS Omega* **2021**, *6*, 8598−8604.
(18) Ge, J.; Yin, Y. Responsive Photonic Crystals. *Angew. Chem., Int. Ed.* **2011**, *50*, 1492−1522.
(19) Lai, X.; Ren, Q.; Vogelbacher, F.; Sha, W. E. I.; Hou, X.; Yao, X.; Song, Y.; Li, M. Bioinspired quasi-3D Multiplexed Anti-Counterfeit Imaging *via* Self-Assembled and Nanoimprinted Photonic Architectures. *Adv. Mater.* **2022**, *34*, 2107243.
(20) Hou, J.; Li, M.; Song, Y. Patterned Colloidal Photonic Crystals. *Angew. Chem., Int. Ed.* **2018**, *57*, 2544−2553.
(21) Holtz, J. H.; Asher, S. A. Polymerized Colloidal Crystal Hydrogel Films As Intelligent Chemical Sensing Materials. *Nature* **1997**, *389*, 829−832.
(22) Fu, F.; Shang, L.; Chen, Z.; Yu, Y.; Zhao, Y. Bioinspired Living Structural Color Hydrogels. *Sci. Robot.* **2018**, *3*, No. eaar8580.
(23) Qi, Y.; Niu, W.; Zhang, S.; Wu, S.; Chu, L.; Ma, W.; Tang, B. Encoding and Decoding of Invisible Complex Information in a Dual-Response Bilayer Photonic Crystal with Tunable Wettability. *Adv. Funct. Mater.* **2019**, *29*, 1906799.
(24) Wang, Y.; Cui, H.; Zhao, Q.; Du, X. Chameleon-Inspired Structural-Color Actuators. *Matter* **2019**, *1*, 626−638.
(25) Wang, Y.; Zhao, Q.; Du, X. Inkless Multi-Color Writing and Copying of Laser-Programmable Photonic Crystals. *Mater. Horiz.* **2020**, *7*, 1341−1347.
(26) Sol, J. A. H. P.; Sentjens, H.; Yang, L.; Grossiord, N.; Schenning, A. P. H. J.; Debije, M. G. Anisotropic Iridescence and Polarization Patterns in a Direct Ink Written Chiral Photonic Polymer. *Adv. Mater.* **2021**, *33*, 2103309.
(27) Qin, L.; Gu, W.; Wei, J.; Yu, Y. Piecewise Phototuning of Self-Organized Helical Superstructures. *Adv. Mater.* **2018**, *30*, 1704941.
(28) Li, Z.; Liu, Y.; Marin, M.; Yin, Y. Thickness-Dependent Wrinkling of PDMS Films for Programmable Mechanochromic Responses. *Nano Research* **2020**, *13*, 1882−1888.
(29) Ma, T.; Bai, J.; Li, T.; Chen, S.; Ma, X.; Yin, J.; Jiang, X. Light-Driven Dynamic Surface Wrinkles for Adaptive Visible Camouflage. *Proc. Natl. Acad. Sci. U. S. A.* **2021**, *118*, No. e2114345118.
(30) Arsenault, A. C.; Puzzo, D. P.; Manners, I.; Ozin, G. A. Photonic-Crystal Full-Colour Displays. *Nat. Photonics* **2007**, *1*, 468−472.
(31) Huang, Y.; Li, F.; Qin, M.; Jiang, L.; Song, Y. A Multi-Stopband Photonic-Crystal Microchip for High-Performance Metal-Ion Recognition Based on Fluorescent Detection. *Angew. Chem., Int. Ed.* **2013**, *52*, 7296−7299.
(32) Zhao, Y.; Zhao, X.; Gu, Z. Photonic Crystals in Bioassays. *Adv. Funct. Mater.* **2010**, *20*, 2970−2988.
(33) Kim, J. B.; Chae, C.; Han, S. H.; Lee, S. Y.; Kim, S. H. Direct Writing of Customized Structural-Color Graphics with Colloidal Photonic Inks. *Sci. Adv.* **2021**, *7*, No. eabj8780.
(34) Li, Z.; Fan, Q.; Yin, Y. Colloidal Self-Assembly Approaches to Smart Nanostructured Materials. *Chem. Rev.* **2022**, *122*, 4976−5067.
(35) Wang, Y.; Zhao, Q.; Du, X. Structurally Coloured Contact Lens Sensor for Point-of-Care Ophthalmic Health Monitoring. *J. Mater. Chem. B* **2020**, *8*, 3519−3526.
(36) Fang, Y.; Ni, Y.; Leo, S. Y.; Taylor, C.; Basile, V.; Jiang, P. Reconfigurable Photonic Crystals Enabled by Pressure-Responsive Shape-Memory Polymers. *Nat. Commun.* **2015**, *6*, 7416.
(37) Fu, Q.; Zhu, H.; Ge, J. Electrically Tunable Liquid Photonic Crystals with Large Dielectric Contrast and Highly Saturated Structural Colors. *Adv.Funct.Mater.* **2018**, *28*, 1804628.
(38) Chen, K.; Fu, Q.; Ye, S.; Ge, J. Multicolor Printing Using Electric-Field-Responsive and Photocurable Photonic Crystals. *Adv. Funct. Mater.* **2017**, *27*, 1702825.
(39) Yu, Z.; Wang, C.-F.; Ling, L.; Chen, L.; Chen, S. Triphase Microfluidic-Directed Self-Assembly: Anisotropic Colloidal Photonic Crystal Supraparticles and Multicolor Patterns Made Easy. *Angew. Chem., Int. Ed.* **2012**, *51*, 2375−2378.
(40) Li, Z.; Qian, C.; Xu, W.; Zhu, C.; Yin, Y. Coupling Morphological and Magnetic Anisotropy for Assembling Tetragonal Colloidal Crystals. *Sci. Adv.* **2021**, *7*, No. eabh1289.
(41) Ge, J.; Yin, Y. Magnetically Responsive Colloidal Photonic Crystals. *J. Mater. Chem.* **2008**, *18*, 5041.
(42) He, L.; Wang, M.; Ge, J.; Yin, Y. Magnetic Assembly Route to Colloidal Responsive Photonic Nanostructures. *Acc. Chem. Res.* **2012**, *45*, 1431−1440.
(43) Liu, Y.; Fan, Q.; Zhu, G.; Shi, G.; Ma, H.; Li, W.; Wu, T.; Chen, J.; Yin, Y.; Guan, J. A Dual Responsive Photonic Liquid for Independent Modulation of Color Brightness and Hue. *Mater. Horiz.* **2021**, *8*, 2032−2040.
(44) Wang, M.; Yin, Y. Magnetically Responsive Nanostructures with Tunable Optical Properties. *J. Am. Chem. Soc.* **2016**, *138*, 6315−6323.
(45) Du, X.; Cui, H.; Xu, T.; Huang, C.; Wang, Y.; Zhao, Q.; Xu, Y.; Wu, X. Reconfiguration, Camouflage, and Color-Shifting for

https://doi.org/10.1021/acsnano.3c00467
ACS Nano 2023, 17, 10269−10279

Bioinspired Adaptive Hydrogel-Based Millirobots. *Adv. Funct. Mater.* **2020**, *30*, 1909202.
(46) Hu, Z.; Lu, X.; Gao, J. Hydrogel Opals. *Adv. Mater.* **2001**, *13*, 1708−1712.
(47) Wang, Y.; Zhang, Z.; Chen, H.; Zhang, H.; Zhang, H.; Zhao, Y. Bio-Inspired Shape-Memory Structural Color Hydrogel Film. *Sci. Bull.* **2022**, *67*, 512−519.
(48) Froyen, A. A. F.; Debije, M. G.; Schenning, A. P. H. J. Polymer Dispersed Cholesteric Liquid Crystal Mixtures for Optical Time-Temperature Integrators. *Adv. Opt. Mater.* **2022**, *10*, 2201648.
(49) Kim, J. W.; Oh, Y.; Lee, S.; Kim, S. H. Thermochromic Microcapsules Containing Chiral Mesogens Enclosed by Hydrogel Shell for Colorimetric Temperature Reporters. *Adv. Funct. Mater.* **2022**, *32*, 2107275.
(50) Lee, S. Y.; Lee, J. S.; Kim, S. H. Colorimetric Recording of Thermal Conditions on Polymeric Inverse Opals. *Adv. Mater.* **2019**, *31*, No. 1901398.
(51) Peng, W.; Zhang, G.; Zhao, Q.; Xie, T. Autonomous Off-Equilibrium Morphing Pathways of a Supramolecular Shape-Memory Polymer. *Adv. Mater.* **2021**, *33*, No. 2102473.
(52) Zhang, X.; Ran, Y.; Fu, Q.; Ge, J. Ultrafast and Irreversibly Thermochromic SiO_2 -PC/PEG Double Layer for Green Thermal Printing. *Small* **2022**, *18*, No. 2106533.
(53) Stöber, W.; Fink, A.; Bohn, E. Controlled Growth of Monodisperse Silica Spheres in the Micron Size Range. *J. Colloid Interface Sci.* **1968**, *26*, 62−69.
(54) Li, Y.; Fan, Q.; Wang, X.; Liu, G.; Chai, L.; Zhou, L.; Shao, J.; Yin, Y. Shear-Induced Assembly of Liquid Colloidal Crystals for Large-Scale Structural Coloration of Textiles. *Adv. Funct. Mater.* **2021**, *31*, 2010746.
(55) Yang, D.; Ye, S.; Ge, J. Solvent Wrapped Metastable Colloidal Crystals: Highly Mutable Colloidal Assemblies Sensitive to Weak External Disturbance. *J. Am. Chem. Soc.* **2013**, *135*, 18370−18376.
(56) Lee, Y. J.; Braun, P. V. Tunable Inverse Opal Hydrogel pH Sensors. *Adv. Mater.* **2003**, *15*, 563−566.
(57) Lüsse, S.; Arnold, K. The Interaction of Poly(Ethylene Glycol) with Water Studied by 1H and 2H NMR Relaxation Time Measurements. *Macromolecules* **1996**, *29*, 4251−4257.
(58) Zhu, B.; Fu, Q.; Chen, K.; Ge, J. Liquid Photonic Crystals for Mesopore Detection. *Angew. Chem., Int. Ed.* **2018**, *57*, 252−256.
(59) Zhang, Y.; Fu, Q.; Ge, J. Photonic Sensing of Organic Solvents Through Geometric Study of Dynamic Reflection Spectrum. *Nat. Commun.* **2015**, *6*, 17510.
(60) Liu, Y.; Han, X.; He, L.; Yin, Y. Thermoresponsive Assembly of Charged Gold Nanoparticles and Their Reversible Tuning of Plasmon Coupling. *Angew. Chem., Int. Ed.* **2012**, *51*, 6373−6377.
(61) Navrotskaya, A.; Aleksandrova, D.; Chekini, M.; Yakavets, I.; Kheiri, S.; Krivoshapkina, E.; Kumacheva, E. Nanostructured Temperature Indicator for Cold Chain Logistics. *ACS Nano* **2022**, *16*, 8641−8650.
(62) *COVID-19 Vaccination: Supply and Logistics Guidance: Interim Guidance*; World Health Organization & United Nations Children's Fund (UNICEF), 12 February 2021.
(63) Hicks, M.; Hing, A.; Gao, L.; Ryan, J.; MacDonald, P. S. Organ Preservation. *Transplant. Immunol.* **2006**, *333*, 331−373.
(64) Xue, j.; Zou, Y.; Deng, Y.; Li, Z. Bioinspired sensor system for health care and human-machine interaction. *EcoMat* **2022**, *4*, No. e12209.
(65) Nie, M.; Huang, C.; Du, X. Recent advances in colour-tunable soft actuators. *Nanoscale* **2021**, *13*, 2780−2791.
(66) Wang, F.; Liu, M.; Liu, C.; Huang, C.; Zhang, L.; Cui, A.; Hu, Z.; Du, X. Light control of droplets on photo-induced charged surfaces. *Natl. Sci. Rev.* **2023**, *10*, nwac164.
(67) Wang, F.; Liu, M.; Liu, C.; Zhao, Q.; Wang, T.; Wang, Z.; Du, X. Light-induced charged slippery surfaces. *Sci. Adv.* **2022**, *8*, No. eabp9369.

https://doi.org/10.1021/acsnano.3c00467
ACS Nano 2023, 17, 10269−10279